Received: 8 December 2020 | Revised: 25 January 2021 | Accepted: 26 January 2021

DOI: 10.1002/jbio.202000479

FULL ARTICLE

JOURNAL OF BIOPHOTONICS

Ex vivo three-dimensional elemental imaging of mouse brain tissue block by laser-induced breakdown spectroscopy

Qingyu Lin[1] | Shuai Wang[2] | Yixiang Duan[1*] | Valery V Tuchin[3,4,5]

[1]School of Mechanical Engineering, Research Center of Analytical Instrumentation, Sichuan University, Chengdu, China

[2]Kunming Institute of Physics, Kunming, China

[3]Research-Educational Institute of Optics and Biophotonics, Saratov State University, Saratov, Russia

[4]Laboratory of Laser Diagnostics of Technical and Living Systems, Institute of Precision Mechanics and Control of the RAS, Saratov, Russia

[5]Interdisciplinary Laboratory of Biophotonics, Tomsk State University, Tomsk, Russia

***Correspondence**
Yixiang Duan, School of Mechanical Engineering, Research Center of Analytical Instrumentation, Sichuan University, 610064 Chengdu, China.
Email: yduan@scu.edu.cn

Funding information
Government of the Russian Federation Grant, Grant/Award Number: 075-15-2019-1885; Natural Science Foundation of China, Grant/Award Number: 61605134; Sichuan Applied Basic Research Project, Grant/Award Number: 2019YJ0078

Abstract

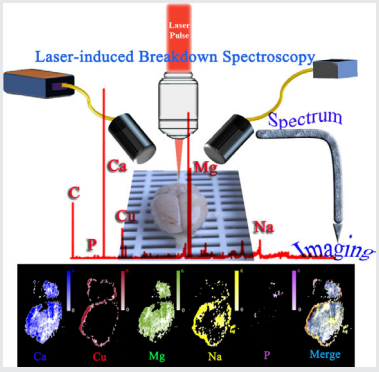

Measurement and reconstruction of an elemental image of large brain tissue will be beneficial to the diagnosis of neurological brain diseases. Herein, laser-induced breakdown spectroscopy (LIBS) is introduced for three dimensional (3D) elemental analysis of paraffin-embedded mouse brain tissue blocks. It is used for the first time towards the mapping of mouse brain block samples. A micro-LIBS prototype is developed for brain elemental imaging and a layer-by-layer approach is used to reconstruct the 3D distribution of Ca, Mg, Na, Cu, and P in the brain tissue. Images are captured with 50 μm lateral resolution and 300 μm depth resolution. The images show that the reclamation area of the cortex surface is enriched with Ca and Mg. In contrast, the Cu distribution is circular and is found primarily in the entirety of the cerebral cortex for the paraffin-embedded brain samples. Elemental imaging results suggest that the highest P intensity is found in the cerebellum nearby the middle sagittal plane in the left-brain paraffin block. These preliminary results indicate that LIBS is a potentially powerful tool for elemental bioimaging of the whole brain and may further improve the understanding of complex brain mechanisms.

KEYWORDS

elemental imaging, ex vivo, laser-induced breakdown spectroscopy, tissue, whole brain

1 | INTRODUCTION

Certain elements play a crucial role in biological systems and processes.[1] In recent decades, there has been an increasing interest in the analysis of elemental distribution and the biochemical significance regarding disease diagnosis.[2] Various analytical methods are used to image elements in biological samples. Nondestructive techniques used to determine elemental distribution in biological samples include particle-induced X-ray emission,[3] micro X-ray fluorescence,[4] energy-dispersive X-ray spectroscopy,[5] and high-resolution synchrotron radiation X-ray fluorescence spectrometry.[6] X-ray-based imaging technologies are major tools for the elemental imaging of tissues. The thermodynamics and kinetics of elements can be also evaluated using membrane diffusible fluorescent probes.[7] Laser ablation inductively coupled plasma mass spectrometer (LA-ICP-MS) can offer a fast and precise spatially resolved measurement of elements in situ at the trace and ultra-trace level. The use of an ICP-MS instrument equipped with a time of flight mass analyzer offers a great advantage for the visualization of elemental

distributions in rat kidney samples.[8] Pisonero et al. developed an attractive nanosecond LA-ICP-MS system and performed the qualitative elemental distribution of gold nanoparticles (NPs) and Cd-based quantum dots within single cells.[9] Although the microprobe X-ray imaging methods have low sensitivity, synchrotron radiation X-ray fluorescence imaging can provide high sensitivity and resolution.[10] Moreover, LA-ICP-MS enables the identification of isotopes in certain conditions and may be more sensitive.[10] However, the complexity of the equipment results in difficulties in applying these methods for routine investigations in research laboratories.[11]

These issues can be mitigated using laser-induced breakdown spectroscopy (LIBS), which is employed to detect elements simultaneously on any sample type using a single laser shot as a micro-destructive analytical technique.[12] The LIBS technique has an excellent capacity to perform sample analysis at the micrometer-scale, making it powerful in surface imaging analysis.[13] Gimenez et al. demonstrated that LIBS imaging can be used for the three dimensional (3D) imaging of nanoparticle distribution in biological tissue with a "layer by layer" analysis.[14] LIBS is suitable for label-free and fast analysis of biological tissue and represents a promising and powerful approach for preclinical investigations.

Currently, LIBS imaging has been used to analyze the distribution of Gd-based drugs and NPs in biological tissue.[15] The distribution of AuNPs[16] in paraffin-embedded tumor tissues was recently investigated using LIBS. The human tumor samples were also studied to demonstrate the mapping functionality of the LIBS technique.[17, 18] When compared with other ablation techniques, such as LA-ICP-MS, LIBS can be used to map major organic elements that were not previously accessible (e.g., C, O, H, and P) in biological tissues.[17] Furthermore, LIBS can be operated quickly as atomization and excitation steps occur simultaneously using single laser pulses.[19]

Metal ions are assumed to contribute to the pathophysiology of neurodegenerative diseases such as Parkinson's and Alzheimer's disease.[20] For instance, the apparent increase in Zn, Cu, Fe, and Ca was found in human plaque of Alzheimer's disease patients in comparison to healthy subjects.[21] Iron is also highly concentrated in neuromelanin is suspected of being a cellular susceptibility factor in Parkinson's disease.[22] Neurodegenerative diseases are known to be correlated with a disturbed distribution of these elements.[23] Therefore, identifying the spatial distribution of elements is crucial for the study of neurological diseases, and measuring elemental distribution in brain tissues is one of the most challenging problems in biomedicine.[24] It is also helpful to monitor the restorative function of sleep to eliminate neurotoxic waste products that accumulate in the awake central nervous system.[25] Currently, measurements of the elemental distribution in brain tissues are performed on a 5 to 20 μm thick slice. Studies always pay attention to a small special function region such as the hippocampus, corpus callosum, or the substantia nigra.[26] Becker et al. stated that a primary issue in brain imaging is to improve the spatial resolution for single-cell analysis, even cell organelles.[27] Measurement and reconstruction of an elemental image of large brain tissue will be beneficial to the diagnosis of neurological brain diseases. Therefore, we aimed to establish a fast and wide-field imaging system that could gain a better understanding of the relationship between elemental distribution and mammalian brain function. Here, 3D elemental imaging of mouse brain tissues using LIBS is demonstrated. A LIBS analytical protocol and experimental setup were proposed for the first time to image the 3D spatial distribution of Ca, Mg, Na, Cu, and P across the brain tissue block.

2 | EXPERIMENTAL SECTION

Figure 1A and Figure 1B are the schematic diagrams of the LIBS experimental setup. A Nd: YAG laser (Innolas, Germany) was employed for producing radiation pulses at 1064 nm and 5 Hz repetition rate with pulse energy adjustable from 1.5 mJ to 100 mJ. Laser pulses were vertically focused onto the sample surface through an apochromatic objective lens (f = 40 mm). The plasma emission was collected using an optical fiber at 45° angle relative to the laser spot and guided into a Czerny-Turner multi-spectrometer (Avantes, Netherlands), and the detection range of 180 to 600 nm was reached with a spectral resolution around 0.15 nm. The spectrometer was synchronized with the Q-switch of the pulse laser. The 2.0 μs was optimized as the optimal delay time. During the experiments, the sample could be translated along three axes by an XYZ motorized stage with a travel distance of 100 mm in each direction, a maximum speed of 10 mm/s and a precision of 5 μm. The XYZ stage was operated at external triggering mode and the movement of the sample was synchronized with the laser firing. A C# software was developed to control the XYZ stage, including the speed and distance adjustment. The vertical positioning of the sample was controlled using a laser pointer and defined before the mapping was performed. The position of the laser pointer (532 nm) on the sample surface, imaged by a compact CCD camera, was indeed direct monitoring of the focusing distance. The position of the Z-stage will not be moved during the LIBS mapping experiment and the ablating point. The measurements were conducted at room temperature and under ambient pressure conditions. A LED lighting the sample

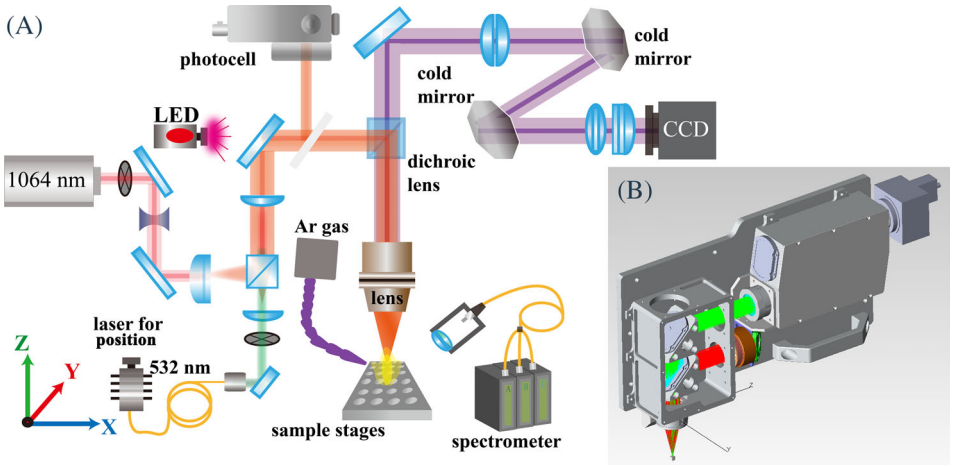

FIGURE 1 Schematic diagram of brain elemental imaging LIBS experimental setup. A, LIBS setup; B, 3D model of the Micro-LIBS prototype. LIBS, laser-induced breakdown spectroscopy

surface allows the operator to choose the shot position through a video of the compact CCD. The photocell outputs a trigger pulse signal to achieve the synchronization between the laser beam and spectrometer. An argon flow (5 L/min) blowing through the plasma was constantly applied among the analysis. The gas was used to prevent surface contamination by ablated particle deposition of the previous laser shots and also to obtain a better sensitivity.[28] Before the brain sample analysis, LIBS experiments were firstly performed on a monocrystalline wafer sample. The Si spectra were used as standard signals to indicate the stability of the experimental setup and keep the consistency of Si spectral signals for each time.

A single emission line was selected for each element of interest, and background correction was performed for every peak. The background correction was performed using custom software and a baseline was defined in the selected wavenumber range. The MATLAB algorithm detected given peaks and defined a baseline in the selected range. LIBS spatial distribution images were reconstructed using the normalized peak area of analytical lines, including the area from 279 nm to 280 nm for Mg (I) 279.8 nm, 393 nm to 394 nm for Ca (I) 393.37 nm, 588.8 nm to 589.2 nm for Na (I) 588.99 nm, 324.6 nm to 324.9 nm for Cu (I) 324.75 nm and 214.23 nm to 214.48 nm for P (I) 214.37 nm. The spectra matrix was displayed using a false-color scale to provide a visual result of the multi-elemental mapping (MATLAB 2018b), expressed in arbitrary units from blue (low distribution) to red or yellow (high distribution).

In the present study, the 8-week-old female mouse brain samples were used as test samples. All the animal experiments were approved by the Ethical Review Committee of Sichuan University. The left-brain and right-brain tissue blocks are shown in Figure 2A and Figure 2B. The brain samples were embedded in paraffin wax with the sagittal view (see Figure 2D and Figure 2E). The LIBS scanning

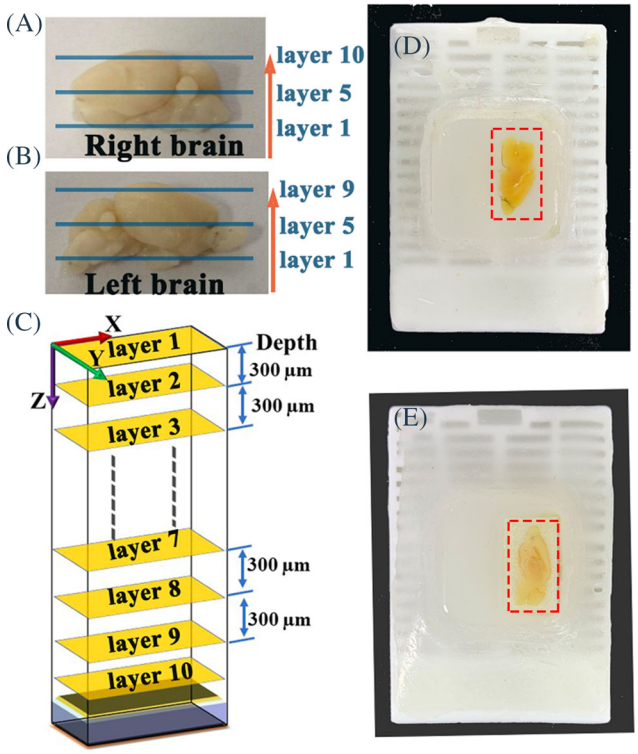

FIGURE 2 The brain tissue block samples and layer-by-layer mapping analysis. A, Right brain tissue block. B, Left brain tissue block. C, LIBS analyze layer-by-layer. D, Paraffin-embedded brain sample before mapping analysis. E, Paraffin-embedded brain sample after mapping analysis. LIBS, laser-induced breakdown spectroscopy

(with a step size of 100 μm) was performed point by point to obtain imaging of elemental distribution. Figure 2C shows the process of LIBS analyze layer-by-layer. The plasma spectrum was recorded for each sampling position. The paraffin-embedded samples were directly scanning analyzed rather than used a thin section of brain tissue, which is more suitable with the advantage of minimal sample preparation of LIBS technique. The analyze region of LIBS

mapping was set within 6 mm × 11 mm area for right-brain, 6 mm × 13 mm area for left-brain, to ensure that the brain tissue block volume was covered (Figure 2E).

The ablated surface of the tissue was subsequently trimmed by microtome to create a fresh flat surface. The depth of trimmed was equal with the ablated depth and ensure the analysis of the next layer will not be affected. Depth of ablated crater was detected with a 3D Optical Microscopes (Contour GT-K, Bruker Nano Inc.). The surface of the ablated crater was measured via Scanning Electron Microscopy (SEM) (JSM-7500F, Oxford Instruments). Sets of consecutive ablation scans, layer by layer, were performed, with 264 000 and 280 800 laser pulses for right-brain and left-brain, respectively. The 3D images were reconstructed based on the results of layer by layer analysis. The time required to analyze each layer imaging was about 1.5 hours at a 5 Hz laser repetition rate. The serial 2D images acquired by LIBS were converted to step-through videos by ImageJ for 3D visualization.

3 | RESULTS AND DISCUSSION

It is well understood that laser pulse energy has a direct influence on the spectral intensity and the size of the ablation craters produced. During LIBS mapping, the ablation crater size contributes directly to the image resolution. Smaller ablation craters result in smaller pixel sizes in the elemental image. However, the emission line intensity is strongly dependent on the amount of ablated material. Therefore, an adequate balance between spatial resolution and detection sensitivity is required.[11] The relationship between laser pulse energy and ablation crater diameter was studied by generating an array of ablation sites with energy between 1.5 and 100 mJ. As expected, the crater diameter increased with increased laser energy (Figure 3A), specifically, the diameter increased from 20 μm to 140 μm. Notably, as shown in Figure 3B, the spectral line intensity increased sharply with laser energy between 1.5 mJ and 10 mJ. When the energy was increased further, the plasma shielding effect prevents efficient ablation of the target material, resulting in poor repeatability.[29] Although the 10 mJ laser-produced higher line intensity, a bigger ablated crater was formed on the paraffin block compared with the 7 mJ laser. Thus, a 7 mJ laser was selected for the following brain elemental distribution experiments to keep a balance between mapping resolution and spectral intensity. The morphology (Figure 3C) and depth profiles of the ablation craters were further characterized using a 3D optical microscope. The results show that the average z-

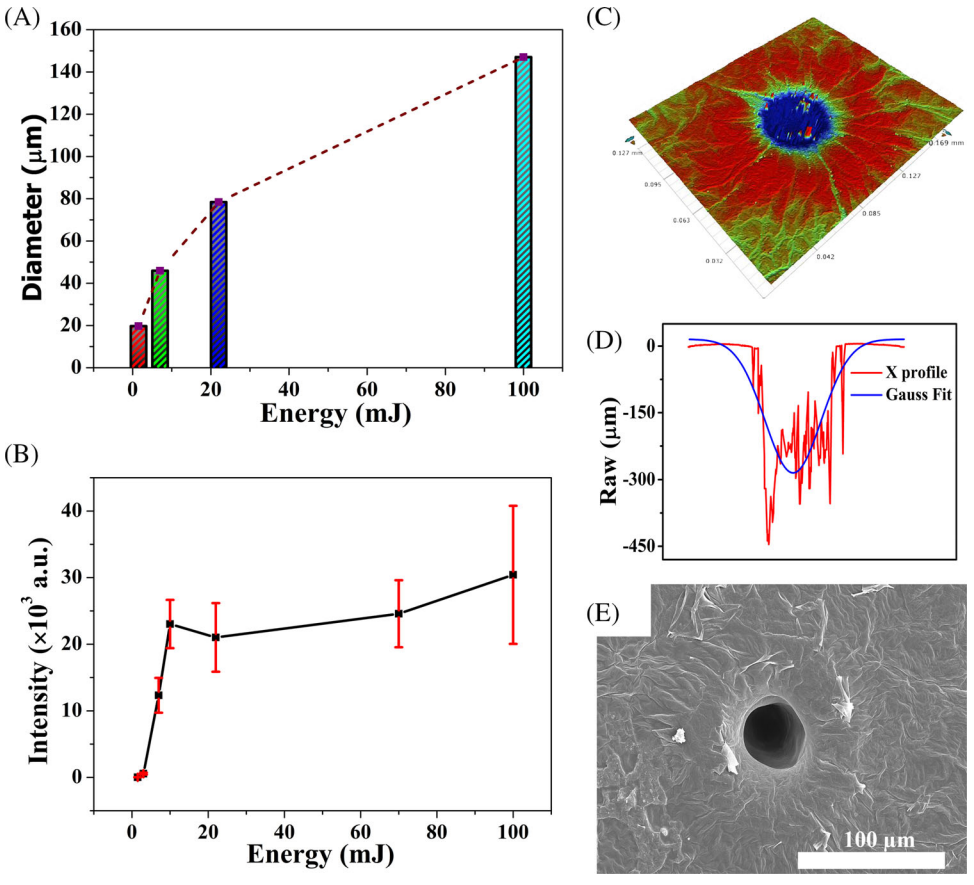

FIGURE 3 Performance of brain elemental imaging LIBS analysis. A, Diameter of ablation crater with different laser energy. B, LIBS emission line intensity for the 247.85 nm Carbon line measured in paraffin sample with different laser energy. C, 3D image of crater measured with the white-light interferometer. D, Depth of ablated crater detected with 3D optical microscopes. E, Surface of crater measured via SEM. LIBS, laser-induced breakdown spectroscopy

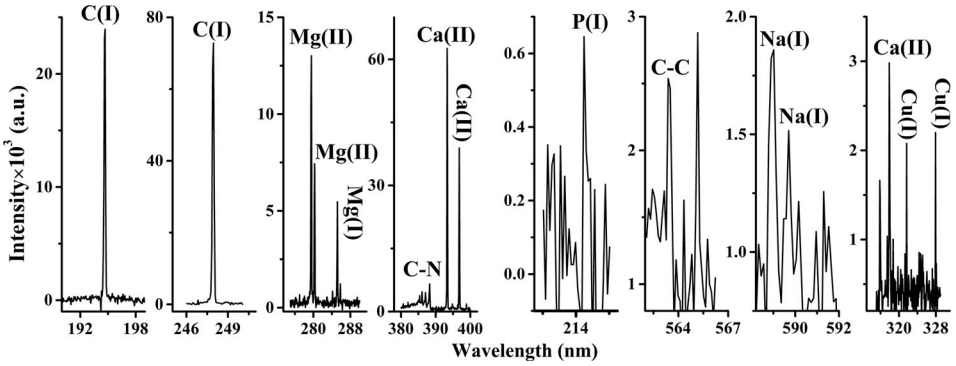

FIGURE 4 LIBS spectra of the paraffin-embedded brain tissue. LIBS, laser-induced breakdown spectroscopy

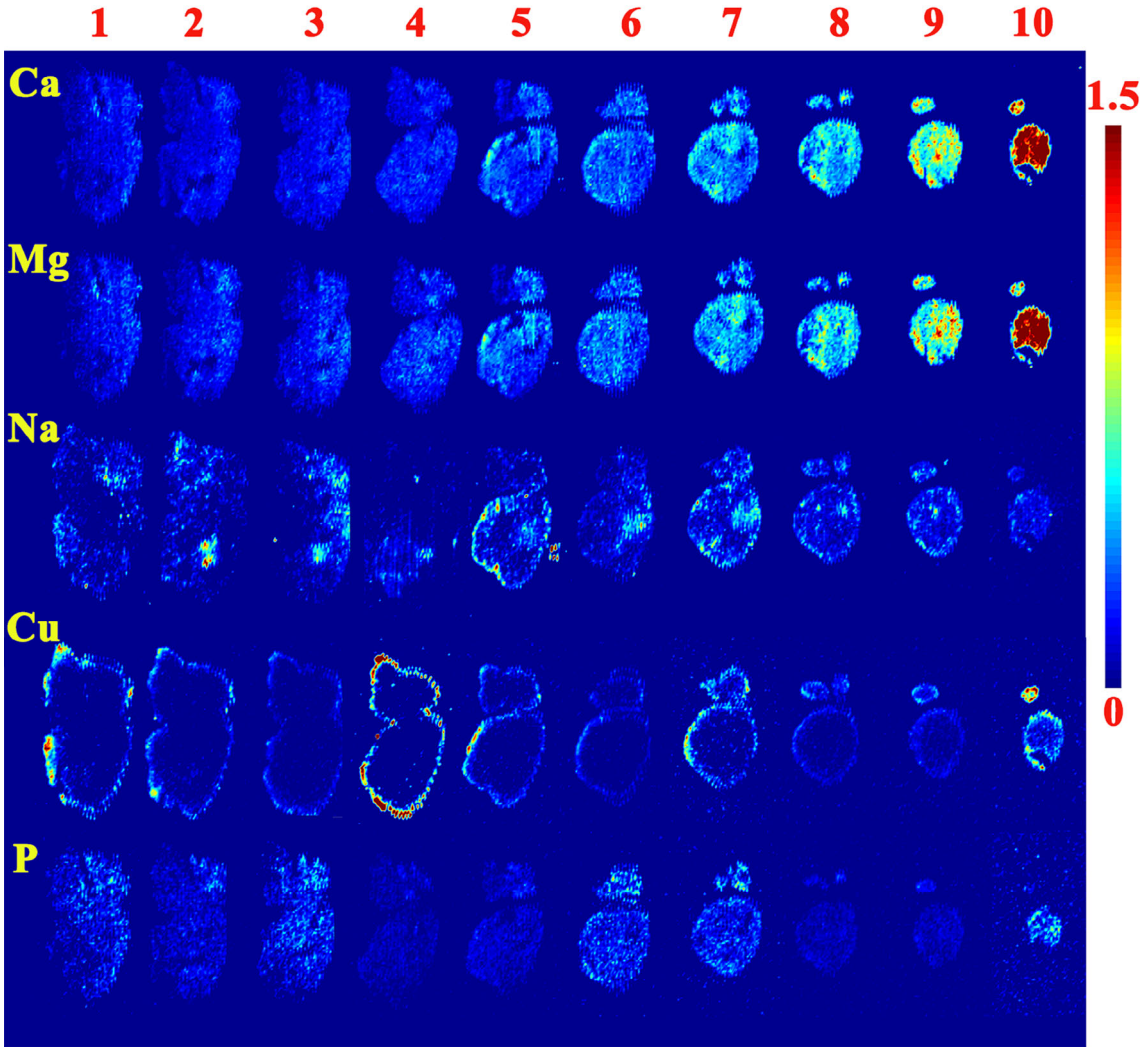

FIGURE 5 Elemental imaging of Ca, Mg, Na, Cu and P in the right-brain tissue block. The color number scale of the elemental images is expressed in arbitrary units. The scale bar means normalized peak area of characteristic lines

depth during LIBS mapping of paraffin brain tissue was 300 μm in our experiment (standard deviation 15 μm, Figure 3D). The configuration and experimental conditions produced ablation craters with 50 μm diameter (Figure 3E).

The LIBS spectra of brain tissue from 180 to 600 nm are shown in Figure 4. Abundant emission lines were identified in this spectral range, including Mg (279.8 nm, 280.27 nm, 285.21 nm), Ca (315.88 nm, 317.93 nm, 321.52 nm, 393.37 nm, 396.85 nm), Na (588.99 nm,

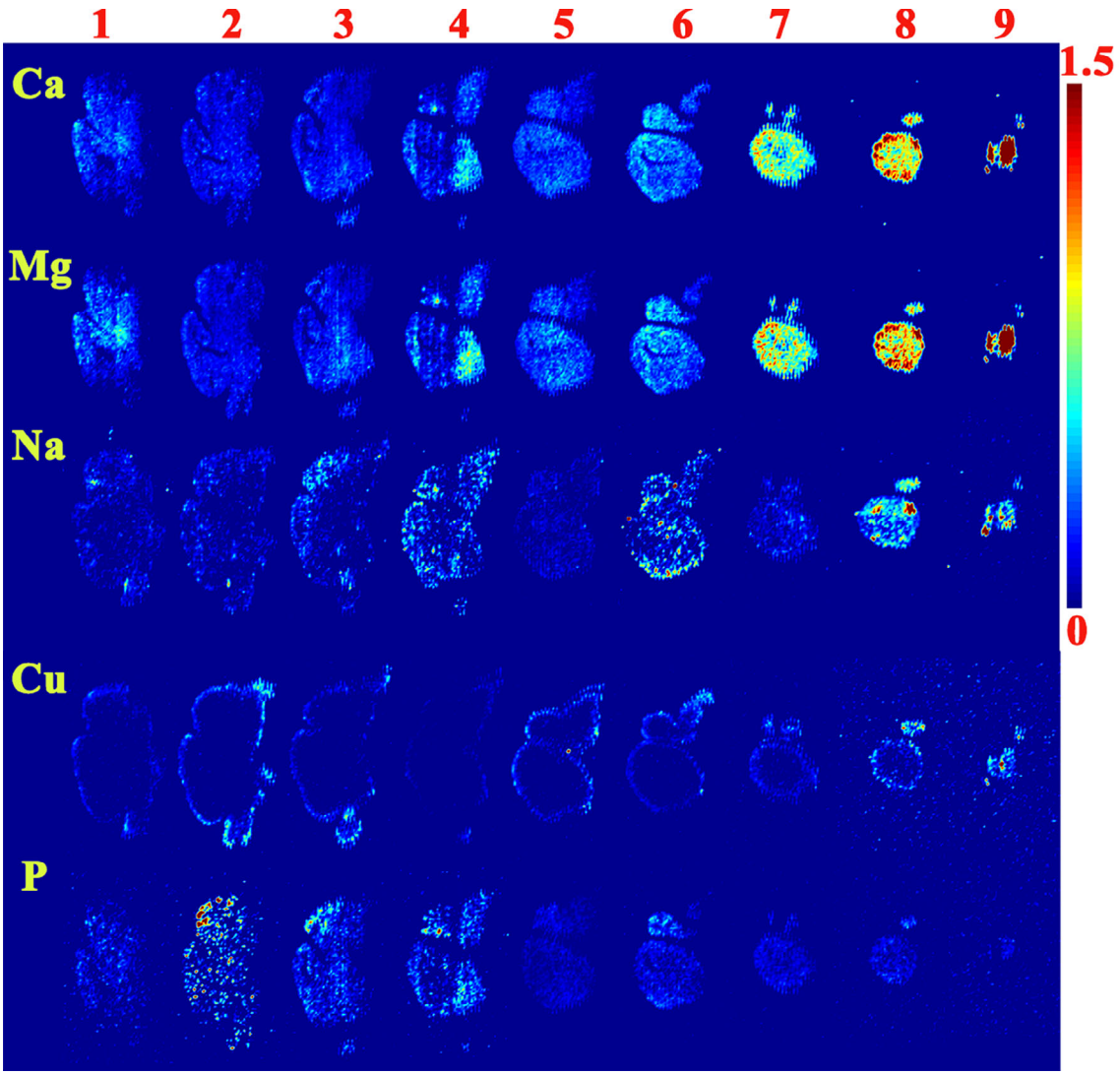

FIGURE 6 Elemental imaging of Ca, Mg, Na, Cu and P in the left-brain tissue. The scale bar means normalized peak area of characteristic lines

589.59 nm), Cu (324.75 nm, 327.4 nm), C (193.09 nm, 247.85 nm) and P (214.37 nm). The LIBS spectra indicate that these elements show an acceptable signal-to-noise ratio. Moreover, the observation of strong C-C (388.34 nm) and C-N (563.55 nm) emission bonds were expected owing to the organic, biological structure of the tissues and the paraffin substrate. C-C and C–N can be observed in LIBS spectra in addition to atomic emission for samples that contain C and N.[30, 31]

The results of elemental imaging using LIBS are shown in Figure 5 (right-brain) and Figure 6 (left-brain). The different analytical layers were represented by the corresponding number. The middle sagittal plane was the first layer analyzed, which is represented by number 1, defined as layer 1. The number 10 in Figure 5 and the number 9 in Figure 6 represent the outermost sagittal layer of the right and left-brain, respectively. The images illustrate the spatial distribution of elements over large areas at brain tissue block. We observe a strong spatial heterogeneity of the elements found in the whole brain block. The image profiles show that Ca and Mg distribute similarly. An apparent increase was observed from the middle sagittal plane to the outermost sagittal layer. Ca and Mg were mostly found in the last three ablated layers, suggesting that the cortex reclamation area was enriched with Ca and Mg. Furthermore, the greatest peak intensities of Ca and Mg in the cerebral cortex were in the auditory and somatosensory cortex. In the cerebellum, the simple lobule, crus of the ansiform lobule, and the paramedian lobule were enriched with Ca and Mg. Otherwise, the cerebral hemisphere cortex exhibited a greater intensity than the cerebellum. It is known that the largest number of neurons are found in

the cerebral cortex, and both elements perform similar functions in the brain and neurons.[32] Thus, a large distribution of Ca and Mg were found in the mouse brain. 3D distributions of Ca and Mg are shown in Visualization S1 and Visualization S2, respectively.

The Na intensity was lower throughout the brain, and the spectra in Figure 5 and Figure 6 indicates that it is heterogeneity distributed. Na is commonly found in biological tissues. However, it was difficult to identify a specific distribution of Na in this work. The Na concentration in the eight-week-old mouse brain was in low-ebb.[33] Although the concentrations of Na in the mouse brain of 8 week-old was low-ebb, it was still higher than Ca and Mg elements.[32] Nonetheless, the Na distribution in the cerebral cortex was lower, compared with that of Ca and Mg, and there was no apparent increase from the middle sagittal layer to the surface sagittal layer. Therefore, the distribution of Na may be severely affected by the paraffin embedding process and clearly showed in the result of the LIBS elemental image. Other authors that studied the trace element analysis by LA-ICP-MS also found that qualitative Na distribution was affected by the paraffin embedding in the cryo-cut tissue.[34] The 3D distribution of Na was reconstructed and shown in Visualization S3.

Cu is an essential element that functions as a cofactor of various enzymes.[24] The Cu distribution forms an enclosed circle all through the whole brain, which suggests that Cu is concentrated in the cerebral cortex. 3D distribution of Cu is shown in Visualization S4. Cu emission lines were weakly detected in the cerebral medulla, attributing to the fact that Cu plays an important role in brain myelination.[35] Circulation and cell metabolism are more active in the cortex,[36] which comprises a thin, wrinkled mantle of gray tissues consisting of millions of neurons. Cu is required for activity, and the oxidative deamination of peptidyl lysine in this region results in the formation of cross-links in collagen and elastin.[37, 38] Furthermore, the spectral intensity of Cu in the right-brain was higher than in the left-brain, specifically in the fourth layer of the right-brain. This was attributed to the appearance of the infralimbic cortex at this depth.

Researchers have reported that nonmetals are mostly found in the corpus callosum.[26, 37] However, here we show that high spectral intensity of P was found in the second, third, and fourth ablated layers of the left-brain within paraffin samples. 3D distribution of P is shown in Visualization S5. The mapping results suggested that P was primarily found around the middle sagittal plane in the left-brain paraffin block. Meanwhile, the highest P intensity was found in the cerebellum nearby the middle sagittal plane.

4 | CONCLUSION

Here, we presented a bioimaging strategy for a mouse brain block tissue based on LIBS. The spatial distribution of Ca, Mg, Na, Cu, and P were evaluated across the brain. For the first time, this methodology demonstrates the possibility of performing ablation-based fast imaging of the mouse brain. The results offer new insight into the use of LIBS for brain tissue elemental imaging. The protocol and device will improve understanding of the chemical basis of many brain diseases. In summary, we have shown that LIBS can be applied for rapid and accurate reconstruction of elemental images across a whole brain. However, further study is required for quantitative analysis and perform mapping towards frozen even fresh brain tissue to avoid analytical bias linked to the FFPE procedures.

ACKNOWLEDGMENTS

The authors are grateful for financial support from the Natural Science Foundation of China (61605134), and the Sichuan Applied Basic Research Project (2019YJ0078). V.V. T was supported by the Government of the Russian Federation Grant No. 075-15-2019-1885. The authors sincerely thank Wenjing Guo for helpful discussions. The authors sincerely thank Long Liang for amending the codes of MATLAB. The authors would like to thank Yu Ding and Chaofan Zhang for their kind help in amending software codes. We thank Fan Bian for thoroughly reviewing the manuscript and thank the help of Prof. Qinghua Zhou on the experiment of 3D Optical Microscopes.

CONFLICTS OF INTEREST

The authors declare no conflict of interests.

AUTHOR CONTRIBUTIONS

The article was written through the contributions of all the authors. All the authors have given approval to the final version of the article.

DATA AVAILABILITY STATEMENT

The data that support the findings of this study are available from the corresponding author upon reasonable request.

ORCID

Qingyu Lin https://orcid.org/0000-0001-9631-5880
Valery V Tuchin https://orcid.org/0000-0001-7479-2694

REFERENCES

[1] R. Lobinski, C. Moulin, R. Ortega, *Biochimie* **2006**, *88*, 1591.
[2] P. Lei, S. Ayton, D. I. Finkelstein, L. Spoerri, G. D. Ciccotosto, D. K. Wright, B. X. Wong, P. A. Adlard, R. A. Cherny, L. Q. Lam, *Nat. Med.* **2012**, *18*, 291.

[3] G. Devès, T. Cohen-Bouhacina, R. Ortega, *Spectrochimica Acta Part B: Atomic Spectroscopy* **2004**, *59*, 1733.
[4] W. Osterode, G. Falkenberg, P. Ferenci, F. Wrba, J. Trace, *Elem. Med. Biol.* **2019**, *51*, 42.
[5] D. E. Newbury, N. W. Ritchie, *Microsc. Microanal.* **2016**, *22*, 520.
[6] A. Ide-Ektessabi, T. Kawakami, R. Ishihara, Y. Mizuno, T. Takeuchi, J. Electron, *Spectrosc. Relat. Phenom.* **2004**, *137*, 801.
[7] L. Yang, R. McRae, M. M. Henary, R. Patel, B. Lai, S. Vogt, C. J. Fahrni, *Proc. Natl. Acad. Sci. U. S. A.* **2005**, *102*, 11179.
[8] O. B. Bauer, O. Hachmöller, O. Borovinskaya, M. Sperling, H. J. Schurek, G. Ciarimbolid, U. Karst, *J. Anal. At. Spectrom* **2019**, *34*, 694.
[9] J. Pisonero, D. Bouzas-Ramos, H. Traub, B. Cappella, C. Álvarez-Llamas, S. Richter, J. C. Mayo, J. M. Costa-Fernandez, N. Bordela, N. Jakubowskic, *J. Anal. At. Spectrom* **2019**, *34*, 655.
[10] B. Busser, S. Moncayo, J. L. Coll, L. Sancey, V. Motto-Ros, *Coord. Chem. Rev.* **2018**, *358*, 70.
[11] L. Sancey, V. Motto-Ros, B. Busser, S. Kotb, J. Benoit, A. Piednoir, F. Lux, O. Tillement, G. Panczer, J. Yu, *Sci. Rep.* **2014**, *4*, 6065.
[12] Q. Y. Lin, G. H. Niu, Q. H. Wang, Q. L. Yu, Y. X. Duan, *Appl. Spectrosc. Rev.* **2013**, *48*, 487.
[13] C. Beresko, P. Kohns, G. Ankerhold, *Spectrochim. Acta, Part B* **2014**, *99*, 20.
[14] Y. Gimenez, B. Busser, F. Trichard, A. Kulesza, J. Laurent, V. Zaun, F. Lux, J. Benoit, G. Panczer, P. Dugourd, *Sci. Rep.* **2016**, *6*, 29936.
[15] A. Detappe, S. Kunjachan, L. Sancey, V. Motto-Ros, D. Biancur, P. Drane, R. Guieze, G. M. Makrigiorgos, O. Tillement, R. Langer, J. Controlled, *Release* **2016**, *238*, 103.
[16] S. Kunjachan, A. Detappe, R. Kumar, T. Ireland, L. Cameron, D. E. Biancur, V. Motto-Ros, L. Sancey, S. Sridhar, G. M. Makrigiorgos, *Nano Lett.* **2015**, *15*, 7488.
[17] M. Bonta, J. J. Gonzalez, C. D. Quarles, R. E. Russo, B. Hegedus, A. Limbeck, *J. Anal. At. Spectrom* **2016**, *31*, 252.
[18] S. Moncayo, F. Trichard, B. Busser, M. Sabatier-Vincent, F. Pelascini, N. Pinel, I. Templier, J. Charles, L. Sancey, V. Motto-Ros, *Acta, Part B* **2017**, *133*, 40.
[19] Q. Lin, P. Yin, Y. Duan, Y. Wang, L. Zhang, X. Wang, *Opt. Express* **2020**, *28*, 14198.
[20] A. Gaeta, R. C. Hider, *B. J. Pharmacol.* **2005**, *146*, 1041.
[21] A. C. Leskovjan, L. AntonioLanzirotti, M. Miller, *Neuroimage* **2009**, *47*, 1215.
[22] C. Depboylu, A. Matusch, F. Tribl, M. Zoriy, P. P. Michel, P. Riederer, M. Gerlach, S. Becker, W. H. Oertel, G. U. Höglinger, *Neurodegener Dis* **2007**, *4*, 218.
[23] C. Grochowski, E. Blicharska, P. Krukow, K. Jonak, M. Maciejewski, D. Szczepanek, K. Jonak, J. Flieger, R. Maciejewski, *Front. Chem.* **2019**, *7*, 115.
[24] J. S. Becker, M. Zoriy, A. Matusch, B. Wu, D. Salber, C. Palm, J. S. Becker, *Mass Spectrom. Rev.* **2010**, *29*, 156.
[25] L. Xie, H. Kang, Q. Xu, M. J. Chen, Y. Liao, M. Thiyagarajan, J. O'Donnell, D. J. Christensen, C. Nicholson, J. J. Iliff, T. Takano, R. Deane, M. Nedergaard, *Science* **2013**, *342*, 373.
[26] M. V. Zoriy, M. Dehnhardt, A. Matusch, J. S. Becker, *Spectrochim. Acta, Part B* **2008**, *63*, 375.
[27] J. S. Becker, *Int. J. Mass Spectrom.* **2010**, *289*, 65.
[28] V. Motto-Ros, L. Sancey, X. Wang, Q. Ma, F. Lux, X. Bai, G. Panczer, O. Tillement, J. Yu, *Spectrochim. Acta, Part B* **2013**, *87*, 168.
[29] C. Aragon, J. A. Aguilera, F. Penalba, *Appl. Spectrosc.* **1999**, *53*, 1259.
[30] L. Feng, J. Wang, H. Li, X. Luo, J. Li, *Anal. Chim. Acta* **2017**, *984*, 66.
[31] M. Dong, J. Lu, S. Yao, Z. Zhong, J. Li, J. Li, W. Lu, *Opt. Express* **2011**, *19*, 17021.
[32] N. C. Spitzer, *Nature* **2006**, *444*, 707.
[33] S. Takahashi, I. Takahashi, H. Sato, Y. Kubota, S. Yoshida, Y. Muramatsu, *Biol. Trace Elem. Res.* **2001**, *80*, 145.
[34] M. Bonta, S. Török, B. Hegedus, B. Döme, A. Limbeck, *Anal. Bioanal. Chem.* **2017**, *409*, 1805.
[35] N. S. Huebner, A. E. Mechling, H. L. Lee, M. Reisert, T. Bienert, J. Hennig, D. Elverfeldt, L. A. Harsan, *Neuroimage* **2017**, *146*, 1.
[36] R. Buxton, K. Uludag, D. Dubowitz, T. Liu, *Neuroimage* **2004**, *23*, 220.
[37] J. R. Prohaska, *Physiol. Rev.* **1987**, *67*, 858.
[38] M. Nickel, C. Gu, *Neural Plast.* **2018**, *2018*, 1.

SUPPORTING INFORMATION

Additional supporting information may be found online in the Supporting Information section at the end of this article.

How to cite this article: Lin Q, Wang S, Duan Y, Tuchin VV. Ex vivo three-dimensional elemental imaging of mouse brain tissue block by laser-induced breakdown spectroscopy. *J. Biophotonics*. 2021;14:e202000479. https://doi.org/10.1002/jbio.202000479